

# Performance Evolution in Satellite Communication Networks Along with Markovian Channel Prediction

Kamal Harb<sup>1,2,\*</sup>, F. Richard Yu<sup>1</sup>, Samir Abdul-Jauwad<sup>2</sup>

<sup>1</sup>Electrical Engineering Department, KFUPM University, Dhahran, 31261, Saudi Arabia

<sup>2</sup>Department of Systems and Computer Engineering, Carleton University, 1125, Colonel By Drive, Ottawa, Ontario, Canada

**Abstract** Augmenting accurate prediction of channel attenuations can be of immense value in improving the quality of signals at high frequency for satellite communication networks. Such prediction of weather related attenuation factors for the impending weather conditions based on the weather data and the Markovian theory are the main object of this paper. The paper also describes an intelligent weather aware control system (IWACS) that is used to employ the predictions made from Markov model to maintain the quality of service (QoS) in channels that are impacted by rain, gaseous, cloud, fog, and scintillation attenuations. Based on that, a three dimensional relationship is proposed among estimated atmospheric attenuations, propagation angle, and predicted rainfall rate ( $RR_{pr}$ ) at a given location and operational frequency. This novel method of predicting weather characteristics supplies valuable data for mitigation planning, and subsequently for developing an algorithm to iteratively tune the IWACS by adaptively selecting appropriate channel frequency, modulation, coding, propagation angle, transmission power level, and data transmission rate to improve the satellite's system performance. Some simulation results are presented to show the effectiveness of the proposed scheme.

**Keywords** Intelligent Weather Aware Control System (IWACS), Markov Model, Quality of Service (QoS), Satellite Communications, Signal to Noise Ratio (SNR), Weather Prediction

## 1. Introduction

Recently, satellite based communication networks at high frequency bands have been rapidly expanding. These high frequency operations have enabled a wide variety of available and potential applications and services including communications, navigation, tele-medicine, remote sensing, distributed sensors networks, and wireless access to the internet. However, high frequency operations are prone to excessive digital transmission errors due to atmospheric attenuations [1]-[8].

Control systems attempt to minimize the effect of attenuation by adjusting the transmission parameters and signal characteristics. However, existing systems rely on total attenuation in actuating the transmission control. Consequently, the control of transmission parameters have been less than the optimal as the detail knowledge of occurrence probabilities for different impairments would have been missing. Knowing expected impairments separately for different attenuation factors, more specifically the weather factors, would help us utilize the most appropriate methods for mitigating impairments with mechanisms like up-link power control, adaptive coding, antenna beam shaping,

antenna diversity [9], [10]. Therefore, improve quality of service (QoS) provisioning [11].

The major atmospheric and weather related factors in signal attenuation are rain fade, gaseous absorption, cloud attenuation, and tropospheric scintillation. Among them, the rain attenuation (RA), also known as rain fade, is the dominant cause of signal impairment, especially at frequencies higher than 10 GHz and small aperture antennas such as Very Small Aperture Terminal (VSAT) and Television Receive Only types (TVRO) [2], [12]-[17].

International Telecommunication Union – Radiocommunications (ITU-R) maintains a large database for probability of precipitation and other parameters. It provides mathematical equations and analytical approaches to estimate rainfall rate (RR) and different atmospheric attenuations around the world from these data [18]. However, ITU-R techniques were developed in view of finding the average conditions and boundary conditions, which are more useful for the design of control system and less for the operation of those systems. Moreover, ITU-R techniques were developed at a time when the high frequency operations above Ku band, where losses become really significant, were not expected. Consequently, there was a great room to first improve the ITU-R techniques to maintain them accurate at higher frequency operations and second, to decouple them from the fifteen years average data provided by ITU-R. Instead, if we make ITU-R techniques work with real-time weather data, those techniques could

\* Corresponding author:

kharb@kfupm.edu.sa (Kamal Harb)

Published online at <http://journal.sapub.org/jwnc>

Copyright © 2012 Scientific & Academic Publishing. All Rights Reserved.

help us achieve better operation, as they were helping us with the system design in the past [13], [14], [17], and [19].

Some of the prior work in the area include [20], where RR is predicted by using weather radar reflection data instead of ground based measurement. Paper [21] presented a method called two level Markov model to predict multi-path fading of signals. Authors of [22] presented a method for RA prediction which yielded good results during low rain and low elevation angle. Authors in [24] presented fade duration prediction as a function of RA and frequency and used modelling of channels to obtain signal attenuation due to clouds and precipitation. While [25] cited difficulty in approximating the losses due to limited availability of experimental data on clouds, [26] cited problem in developing accurate models due to ambiguity of cloud water content and cloud extent limits. In [10], authors present prediction models and analytical techniques for a range of operational parameters involving low-margin, low elevation angle, inclined geosynchronous, and low earth orbit systems. The paper estimated rain and scintillation while assuming gaseous attenuations as constant. These techniques have helped to mature the control systems in satellite communication. Due to new bandwidth and frequency requirements, the problems of attenuations due to various atmospheric factors have come to receive increased level of prominence due to increased operations at frequencies above 10 GHz. These problems are articulated very well by [2], [3], [7], and [12].

In our past research work, we demonstrated that a better control of satellite signal parameters resulting in improved system performance could be achieved by taking into account the major weather related contributors of signal attenuation separately [16]. In [5] we demonstrated how estimation of RR, as well as attenuation due to rain, gas, cloud, fog, and scintillation, could be measured. The methodology yielded greater accuracy in estimating the weather related attenuation. Total attenuation as well as constituent weather attenuations were calculated for any rainfall conditions and for any elevation angle. However, this methodology relied on historical data collected by ITU-R that provided average rainfall per year for locations throughout the world based on statistical data collected over a decade [6]. During the research, we realized that the estimations would have helped tune channel parameters in real-time had the real-time measurements been used to gain a closer estimation of impending weather conditions. The work reported in this paper was inspired by that premise. As research thrusts were put to improve QoS on satellite based networks with the use of intelligent prediction methods, the work presented in this paper should be of significant interest to research and development community. This paper makes four major contributions towards improving the operation of satellite control systems and enhancing the performance of satellite network systems. This is specifically true during severe weather condition and operations of communication channels above Ku band. The major contributions of the work are:

1. Migration of ITU-R techniques from the domain of the improving design to the domain of improving the operation,
2. Application of Markov theory in real-time prediction of weather and applying of those predictions in the forecast of atmospheric attenuation,
3. Improvement of ITU-R techniques in predicting rain, gas, cloud, fog, and scintillation attenuations more accurately at wide range of frequencies including Ka band and to make them work at any propagation angle, and RRs,
4. An enhanced intelligent weather aware control system (IWACS) for achieving improved channel performance.

This paper is presented in five sections. Section 2 describes prediction of different weather attenuation factors based on Markovian modelling of weather characteristics. Section 3 describes calculation of rain, gaseous, cloud, fog, and scintillation attenuations which will be used by IWACS in decision making. Section 4 presents simulation environment and implementation of IWACS, results and discussions. Finally, we conclude this study in Section 5.

## 2. Prediction of Channel Characteristics

This section describes the behaviour of RA at high frequency and proposes a method for better estimating channel attenuation in weather impacted satellite networks. The RA is computed, based on predicted rainfall rate ( $RR_{pr}$ ), which itself is predicted by using Markov theory [27] along with ITU-R models and bi-linear interpolation [28], [29]. The method predicts RR at any location on earth, for a wide range of propagation angles and frequencies. The  $RR_{pr}$  values are then used to adjust the control parameters and, therefore, help improve the QoS in communication channels.

### 2.1. The Rainfall Rate Prediction

In this section, we present prediction of rainfall rate using Markov theory on the time series of weather data. For that reason, weather is considered a discrete random process that can assume a set of finite states. Further, it is assumed that the change from one state to another is a random discrete step with certain transition probability ( $p$ ), whose value is derived from statistical properties of the system.

#### 2.1.1. Classification of Rain

For the purpose of explaining to the reader the application of Markov modelling for predicted rainfall rate, a specific location is chosen where we divided rainfall rate ranges into five classes starting from zero mm/hr up to the highest rainfall rate as follows:

- a. Class A: from zero up to but less than 1 mm/hr.
- b. Class B: from 1 up to but less than 4 mm/hr.
- c. Class C: from 4 up to but less than 8 mm/hr.
- d. Class D: from 8 up to but less than 14 mm/hr.
- e. Class E: values greater than 14 mm/hr.

The discrete time interval chosen in this study was one

hour. The reason being that environment should supply weather data in one hour intervals. However, the method can be applied for finer grain intervals given that weather data for shorter intervals are available.

The approach in grouping total rain conditions into classified blocks has been depicted in Figure 1. This classification in actual data provides the basis for the data required to apply Markovian theory in the prediction of rainfall rate [8].

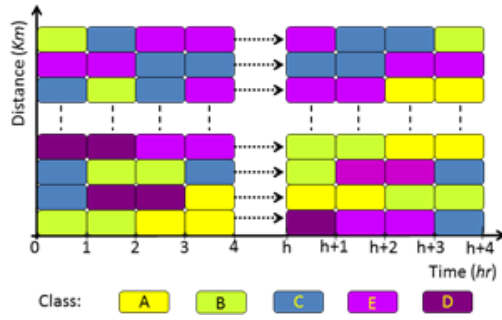


Figure 1. Presentation of the five rainfall rate classes

To make the classification of rainfall rate to better reflect local statistical weather patterns, two parameters can be adjusted:

a. Periodicity of rainfall rate: Instead of selecting one hour interval, periodicity in minutes or hours could be used. The smaller the sampling period, the more instantaneous will be the rainfall rate values especially when dealing with rapidly changing weather conditions.

b. Number of classes: Instead of five, the number of classes could be decreased or increased according to the variation of rainfall rate history for that location. More classes means more computational time with finer granularity of control.

### 2.1.2. Markov Model Implementation

#### I- Weight of Transition Probability Matrices:

Different weights are assigned to each Markov state, zero order (present state), first order (previous state), and second order (previous to previous state), as defined in Markov

Chain theory. There exist no direct formulas for calculating these weights and it needs iterative search involving trial and error. The weight values need to be validated over many sets of data.

The resulting weight vector is denoted as:

$$[W]_{(1 \times 3)} = [W(0) \ W(1) \ W(2)], \quad (1)$$

where  $W(0)$ ,  $W(1)$ , and  $W(2)$  represent weight assigned to present, previous, and previous to previous intervals, respectively, as shown in Figure 2. Each weight in (1) has a different unique value and the largest value will belong to the present weight  $W(0)$  and so on for the other weights. Also, these weights are positive numbers and their summation is equal to one. This research came to conclude that there exists a set of weight that work very well for all possible sets of transition probability matrices describe below.

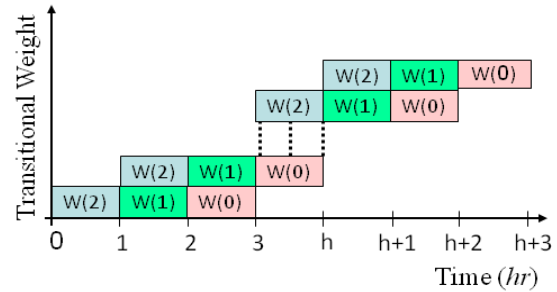


Figure 2. Presentation of the three different weights

#### II- Transition Probability:

The transition probabilities and classification of rain are directly correlated. The transition probabilities are the probabilities of moving from given state to another state.

In Markov Chain theory, the probability of a discrete event to remain in state  $x$  is denoted as  $P(x)$ . In this representation, independent chains without any memory of past state are called zero-order Markov Chains. The transition probability matrix of zero-order Markov Chain theory  $[P_0]$  for the five presented classes is, thus, represented as follows:

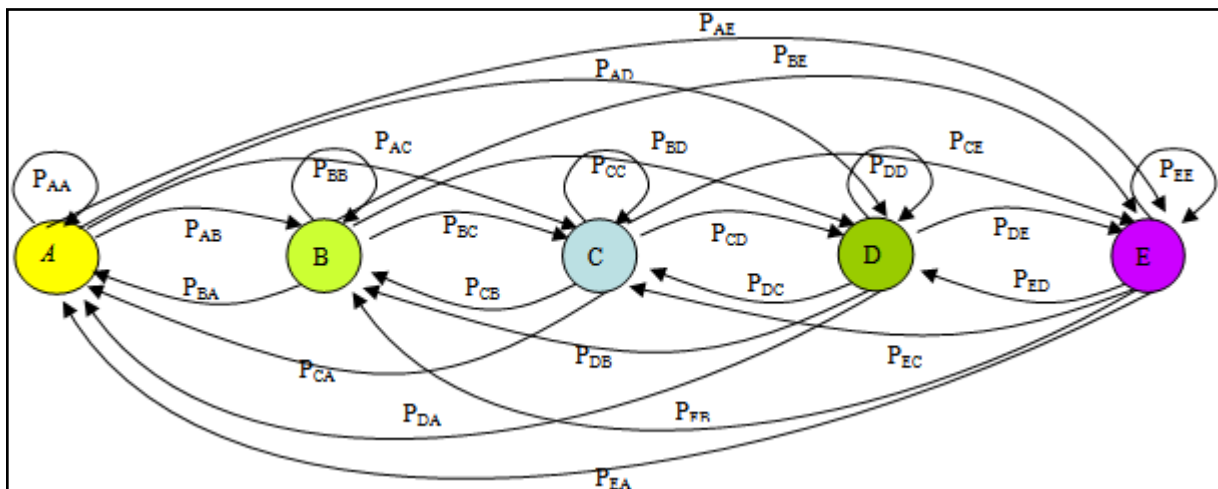


Figure 3. First Order Markov Chain model with transition probabilities for switching among different states

$$[P_0]_{(1 \times m)} = [P_A \ P_B \ P_C \ P_D \ P_E]. \quad (2)$$

Then the process consisting of a finite number of states with known probabilities  $P(x, y)$  of transition from state  $y$  to state  $x$  is considered a first order Markov Chain [27], [30]–[31]. The transition probability matrix of the first-order Markov Chain for the five classes is shown below in (3). These transitions are depicted in a pictorial form in Figure 3 and can be represented by:

$$\begin{bmatrix} P \\ 1 \end{bmatrix}_{(m \times m)} = \begin{matrix} & A & B & C & D & E \\ \begin{matrix} A \\ B \\ C \\ D \\ E \end{matrix} & \begin{bmatrix} P_{AA} & P_{AB} & P_{AC} & P_{AD} & P_{AE} \\ P_{BA} & P_{BB} & P_{BC} & P_{BD} & P_{BE} \\ P_{CA} & P_{CB} & P_{CC} & P_{CD} & P_{CE} \\ P_{DA} & P_{DB} & P_{DC} & P_{DD} & P_{DE} \\ P_{EA} & P_{EB} & P_{EC} & P_{ED} & P_{EE} \end{bmatrix} \end{matrix}. \quad (3)$$

Similarly, the transition probability matrix of the second-order Markov Chain theory  $P(z|xy)$  for the five classes is presented in (4).

$$\begin{bmatrix} P \\ 2 \end{bmatrix}_{(m \times m)} = \begin{matrix} & A & B & C & D & E \\ \begin{matrix} AA \\ AB \\ AC \\ AD \\ AE \\ BA \\ BB \\ BC \\ BD \\ BE \\ CA \\ CB \\ CC \\ CD \\ CE \\ DA \\ DB \\ DC \\ DD \\ DE \\ EA \\ EB \\ EC \\ ED \\ EE \end{matrix} & \begin{bmatrix} P_{AAA} & P_{AAB} & P_{AAC} & P_{AAD} & P_{AAE} \\ P_{ABA} & P_{ABB} & P_{ABC} & P_{ABD} & P_{ABE} \\ P_{ACA} & P_{ACB} & P_{ACC} & P_{ACD} & P_{ACE} \\ P_{ADA} & P_{ADB} & P_{ADC} & P_{ADD} & P_{ADE} \\ P_{AEA} & P_{AEB} & P_{AEC} & P_{AED} & P_{AEE} \\ P_{BAA} & P_{BAB} & P_{BAC} & P_{BAD} & P_{BAE} \\ P_{BBA} & P_{BBB} & P_{BBC} & P_{BBD} & P_{BBE} \\ P_{BCA} & P_{BCB} & P_{BCC} & P_{BCD} & P_{BCE} \\ P_{BDA} & P_{BDB} & P_{BDC} & P_{BDD} & P_{BDE} \\ P_{BEA} & P_{BEB} & P_{BEC} & P_{BED} & P_{BEE} \\ P_{CAA} & P_{CAB} & P_{CAC} & P_{CAD} & P_{CAE} \\ P_{CBA} & P_{CBB} & P_{CBC} & P_{CBD} & P_{CBE} \\ P_{CCA} & P_{CCB} & P_{CCC} & P_{CCD} & P_{CCE} \\ P_{CDA} & P_{CDB} & P_{CDC} & P_{CDD} & P_{CDE} \\ P_{CEA} & P_{CEB} & P_{CEC} & P_{CED} & P_{CEE} \\ P_{DA A} & P_{DAB} & P_{DAC} & P_{DAD} & P_{DAE} \\ P_{DBA} & P_{DBB} & P_{DBC} & P_{DBD} & P_{DBE} \\ P_{DCA} & P_{DCB} & P_{DCC} & P_{DCD} & P_{DCE} \\ P_{DDA} & P_{ddb} & P_{DDC} & P_{DDD} & P_{DDE} \\ P_{DEA} & P_{DEB} & P_{DEC} & P_{DED} & P_{DEE} \\ P_{EAA} & P_{EAB} & P_{EAC} & P_{EAD} & P_{EAE} \\ P_{EBA} & P_{EBB} & P_{EBC} & P_{EBD} & P_{EBE} \\ P_{ECA} & P_{ECB} & P_{ECC} & P_{ECD} & P_{ECE} \\ P_{EDA} & P_{EDB} & P_{EDC} & P_{EDD} & P_{EDE} \\ P_{EEA} & P_{EEB} & P_{EEC} & P_{EED} & P_{EEE} \end{bmatrix} \end{matrix}. \quad (4)$$

The characteristics of these transition probability matrices are such that the entries for each column vectors in (2), (3), and (4) are positive numbers. The sum of the elements of each row in the matrices is one. The columns

represent probability vectors, which are the stochastic values for transition. The transition probabilities are dependent on statistical pattern of rain at a particular geography and climate.

Note that,  $m$  and  $n$  represent the number of rows and columns, respectively.

### 2.1.3. Predicted Rainfall Rate

The value of predicted rainfall rate for the immediately following discrete time period is computed based on probability and weight combinations. These combinations present a special module of weather prediction of different weights assigned to each transition probability matrix along with Markov Chain of order  $\phi$  where  $\phi$  is finite and equal to 2 in our case. Thus, the prediction of the future state is dependent on the present, previous, and previous to previous states and is independent of the other earlier states [8].

Given that the zero  $[P_0]$ , first  $[P_1]$ , and second order  $[P_2]$  transition probability matrices with the weights assigned to each matrix  $(W(0))$ ,  $(W(1))$ , and  $(W(2))$ , respectively. The predicted rainfall rate values can be computed as follows:  
 $PW(1) = W(0).P_0(1) + W(1).P_1(m, 1) + W(2).P_2(n, 1)$   
 $PW(2) = W(0).P_0(2) + W(1).P_1(m, 2) + W(2).P_2(n, 2)$   
 $PW(3) = W(0).P_0(3) + W(1).P_1(m, 3) + W(2).P_2(n, 3)$   
 $PW(4) = W(0).P_0(4) + W(1).P_1(m, 4) + W(2).P_2(n, 4)$   
 $PW(5) = W(0).P_0(5) + W(1).P_1(m, 5) + W(2).P_2(n, 5). \quad (1)$

Where the numbers (1, 2, 3, 4, and 5) represent the five classes (A, B, C, D, and E) shown in Figure 1.

$[P_0]$  represents the row corresponding to the present state.  $[P_1]$  represents the row corresponding to the transition from the last state to the present state.  $[P_2]$  represents the row corresponding to the transition from the last-to-last to the last state and then to the present state. In our specific case, the  $m$  can be any value ranging from 1 to 5 and  $n$  can be any value ranging from 1 to 25 according to the previous and previous to previous weather state, respectively.

Also,  $PW$ s presented in (5) can be written in a simple mathematical form as:

$$PW(u) = W(0).P_0(u) + W(1).P_1(m, u) + W(2).P_2(n, u). \quad (2)$$

Where  $u$  ranges from 1 to 5 and  $PW$  represents the probability weight values of the five existing classes (A, B, C, D, and E), thus:

$$[PW]_{(u \times 1)} = [PW(1) \ PW(2) \ PW(3) \ PW(4) \ PW(5)] \\ = [PW_A \ PW_B \ PW_C \ PW_D \ PW_E]. \quad (3)$$

Therefore, the predicted rainfall rate ( $RR_{pr}$ ) will be belonging to the class that has the maximum probability weight of  $PW$  vector collected from (7).

Figure 4 shows a demonstration for the effectiveness of our method for predicting rainfall rate. At the beginning, we used randomly generated values of rainfall rate to determine the weights and probability matrix elements for our model [15].

These values were then tested against rainfall rate values that were collected by Environment Canada for a almost two month duration at South West of King City using weather radar near Toronto, Ontario, Canada. We applied our methodology to predict the future state out of past states. The

prediction data obtained using our method and the measured rainfall data from Environment Canada are provided in Figure 4 and in Table 1.

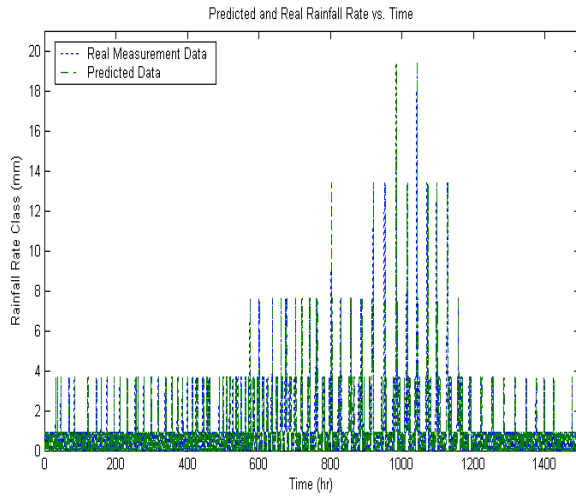


**Figure 4.** Comparison of actual and predicted rainfall rate values at South West of King City

**Table 1.** Comparison of Accurate and Predicted Rainfall Rate Data at Different Time

Time [hr]	Accurate Time Data [mm/hr]	Predicted Data [mm/hr]	Different Between Both Results [mm/hr]
1	0	0	0
3	0	0	0
4	0	0	0
80	0	0	0
170	0	0	0
200	0	0	0
210	1	0	1
220	0	0	0
330	0	0	0
338	1	1	0
350	0	0	0
510	1	1	0
610	1	1	0
620	0	0	0
640	0	0	0
650	1	1	0
780	1	1	0
790	0	0	0
880	1	1	0
890	0	0	0
970	0	0	0
1071	8	8	0
1098	4	4	0
1103	0	1	1
1104	1	1	0
1126	8	4	4
1127	8	8	0
1137	1	1	0
1148	0	0	0
1152	0	0	0
1155	1	1	0
1190	1	1	0
1192	1	1	0
1429	0	0	0

Note that only small numbers of samples are presented in the table to keep it readable and that the prediction matches closely with the measured results.

We conclude that, the Markovian Chain has promising application in effectively predicting the future weather result in statistical terms. The results are astoundingly accurate. Therefore, our methodology for predicting rainfall rate can be applied under different weather conditions at any given location on earth.

#### 2.1.4. The Values of Weights and Transition Probabilities

The values of the weight matrix as defined in (1) and the transition probabilities as defined in (2), (3), and (4) were obtained through an extensive exercise of iterative adjustments and their test of validity on rainfall rate data. At the end, the study not only revealed a set of workable values but they also revealed the following behaviours:

1- For a given set of transition probabilities, there is a corresponding weight that gives the best prediction of rainfall rate in Markov Chain theory.

2- Studies done over actual rain data revealed that the five states model developed here gives extremely reliable prediction of rain with the following values of weights (W's) are:

$$[W]_{(1 \times 3)} = [0.495 \ 0.335 \ 0.170] \quad (8)$$

and transition probabilities (P's) are:

$$[P_0]_{(1 \times 5)} = [0.35 \ 0.25 \ 0.2 \ 0.1 \ 0.1], \quad (9)$$

$$[P_1]_{(1 \times 5)} = \begin{matrix} A & B & C & D & E \end{matrix} \quad (10)$$

$$\begin{matrix} A \\ \vdots \\ E \end{matrix} \begin{bmatrix} 0.43 & 0.33 & 0.2 & 0.04 & 0 \\ \vdots & \vdots & \vdots & \vdots & \vdots \\ P_{EA} & P_{EB} & P_{EC} & P_{ED} & P_{EE} \end{bmatrix}$$

and

$$[P_2]_{(5 \times 25)} = \begin{matrix} A & B & C & D & E \end{matrix} \quad (11)$$

$$\begin{matrix} AA \\ \vdots \\ EE \end{matrix} \begin{bmatrix} 0.45 & 0.37 & 0.14 & 0.03 & 0.01 \\ \vdots & \vdots & \vdots & \vdots & \vdots \\ P_{EEA} & P_{EEB} & P_{EEC} & P_{EED} & P_{EEE} \end{bmatrix}$$

The full set of values could be obtained by contacting the authors.

3- When rain rate classification as done in Section 2.1.1 is altered to better suite different locations on earth, the coefficients mentioned above will change. However, the values listed here will give good starting values for the iterative process of finding the new values.

Notice that, the weights and the transition probability matrices values are selected initially based on the statistical investigation of historical field of data collected over several

years. We discovered that the coefficient of the matrices and the weights remain relatively stable although weather conditions vary significantly. Nevertheless, some severe weather conditions not recorded by the data analysed for this research could require some adjustments.

Note that, we acknowledge the dependence of Markovian theory in stochastic assumptions and the potential errors in estimating the weights and the coefficients of transition probability matrices. This is denoted especially for the fact that the method assumes stationary weather within one discrete time period; its prediction is nothing more than a practical approximation. Nevertheless, the test on the fields' data demonstrated highly respectable results, yielding prediction values to contain low relative percentage error of ( $\leq 9.9\%$ ) for the presented fifteen hundred hours for rainfall rate.

## 2.2. Migrating ITU-R Model from the Design Domain to the Operational Domain

ITU-R technique for estimating environmental attenuations based on weather data collected over a decade and a half has served us well in system design because it is able to provide average and boundary conditions that a communication system would be subjected to. ITU-R provides not only the geographic parameters of a location, such as the height above the sea level and the average rain height as shown in Figure 5, but also the weather factors like probability of precipitation and mathematical formula for estimating rainfall rate, and subsequently estimating signal attenuation due to rain, gas, cloud, fog, and scintillation. The knowledge of the attenuation serves useful purpose in optimizing the design by finding the best combination of frequency, modulation, coding, and other transmission and reception parameters for a given location in relative to other locations.

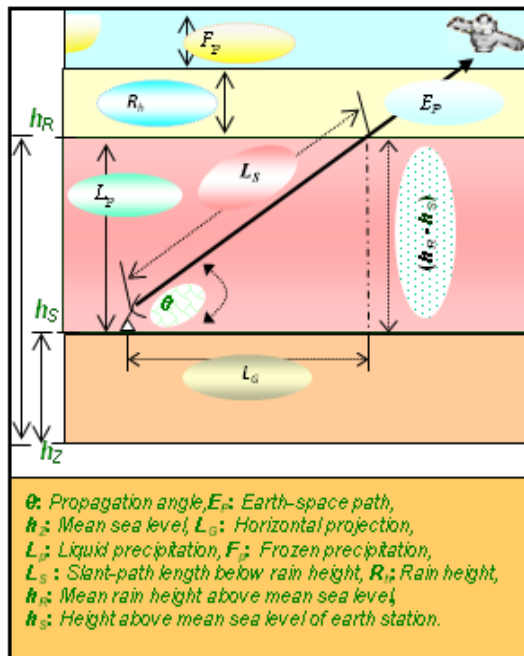


Figure 5. Earth-space path

The research work reported in this paper stemmed from knowing that if these techniques were to be extended to estimate the attenuations in a real-time environment, they would have greatly served in the purpose of operating those designed systems optimally by allowing selecting proper combination of controllable parameters. Therefore, the ITU-R methodology was studied and extended to solve the problem of adapting the control systems with instantaneous variations of weather attenuation.

We propose the use of Markov theory in estimating the weather condition for the immediately following time period based on the real-time data of immediately preceding periods and the statistical probability of state changes. Subsequent experiments demonstrated that the inclusion of Markovian prediction technique and its resulting data as an input to ITU-R techniques resulted in real-time prediction of weather attenuations.

The next enhancement made in ITU-R techniques was estimating attenuation as a function of rainfall rate, propagation angle, and operational frequencies so that they hold true even under high frequency operation above Ku band. The outcome of these changes was that they yielded highly accurate estimation of RR and then that of rain, gaseous, fog, cloud, and scintillation attenuations. Such evolution in the ability to predict weather attenuation in real-time had direct consequence in improving the real-time control by enhancing the ability to select the signal parameters.

The following are the key benefits achieved by the proposed technique:

1. Better estimation of attenuation including high frequency operations.
2. Real-time estimation of RR. The prediction of RR is made by viewing the weather data from a moving window of fixed time intervals and the impending rainfall rate is estimated based on current rate, previous rate, and previous to previous rate.
3. Calculation of attenuations based on the real-time estimation of RR.
4. Real-time signal adaptation to weather variation by selecting appropriate channel parameters.

## 3. Calculation of Rain, Gaseous, Cloud, Fog, and Scintillation Attenuations

In this paper, a new relationship model is proposed for estimating various weather attenuations as a function of propagation angle,  $RR_{pr}$ , and frequency, for any derived geographic location of ground terminals. This model results in three dimensional graphs which relates the attenuation,  $RR_{pr}$ , and propagation angle for a selected operational frequency, which may be any value from 0 to 55 GHz. RA is the single greatest weather dependent signal attenuation factor, which occurs in satellite networks largely due to signal absorption and scattering of incoming signal. Fortunately rain forms only in the troposphere that extends

around sixteen kilometers from sea level while the satellites are located in geostationary orbit at 35,800 km above earth [6]. Therefore, exposing signal to rain attenuation only during a small portion of its transmission path as shown in Figure 6.

Nevertheless as the frequency increase the losses increase as shown in Table 2 [32]-[35]. Even heavy rainfall of 10 cm/hr seems to cause a small attenuation of 0.05 dB/km with RF signals at 2.4 GHz. The Ku band attenuation for the same rainfall, however, is approximately nine times that of C-band, and thus very substantial for it to be ignored [36], [37]. Therefore, estimating different atmospheric attenuations at regional or individual sites is important for improving control of satellite channel parameters especially when higher transmission frequencies are adopted to achieve greater transmission rate through communication channels.

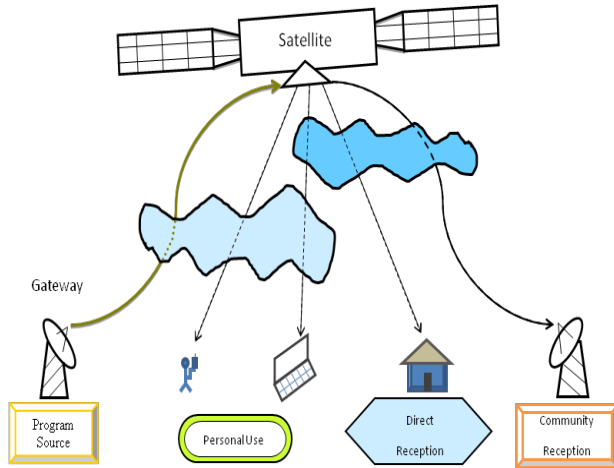


**Figure 6.** A satellite broadcast system in the presence of horrendous weather condition

**Table 2.** VSAT frequency spectrum allocation

Band	Frequency GHz	Area Foot-print	Power Delivered	Rainfall effect
C	3 - 7	Large	Low	Minimum
Ku	10 - 18	Medium	Medium	Moderate
Ka	18 - 31	Small	High	Severe

In this section a new technique for estimating channel attenuation is presented. This technique, estimates constituent contributors of total attenuation separately and extends it to give good approximations for a wide range of signal frequencies, propagation angle, and  $RR_{pr}$ . The technique uses ITU-R coefficients as shown in Figure 5 while estimating the attenuation at grid locations in a weather collection map that was used by ITU-R. In cases where the location of concern does not fall on the grid, a bi-linear interpolation technique is then used to get the parameters [5], [13].

Most of the formulas and variables presented in this section are direct evolutions from the ITU-R method with notify modifications and enhanced presentation for different weather parameters. We implemented these formulas and variables to handle real-time data of the present one hour window and used the Markovian prediction that was

presented earlier with proposed values of the matrices components to predict the data for the following period.

This section is devoted first, to predict constituent contributors of channel attenuation separately due to different weather variants, and then, to determine the total attenuation due to all of the factors combined. Also, included in this section is the technique for calculating the signal to noise ratio (SNR) based on these attenuations.

### 3.1. Calculating Rain Attenuation (RA)

The RA, represented as  $(A_r)$ , is predicted by using a set of functions and solving them for different satellite-location dependent values. The values of RA are calculated as a function of frequency ( $f$ ) and predicted rainfall rate ( $RR_{pr}$ ). The foundational work of this technique and its variables are explained in [5], [14] and [38].

The key destination of this technique is that we start with an attenuation value at a known frequency ( $f_n$ ), and then estimate the attenuation at one increment higher frequency ( $f_{n+1}$ ). Then using the attenuation at ( $f_{n+1}$ ), we find attenuation at ( $f_{n+2}$ ), and so on. That is, once RA is known at any lower frequency, we will be able to compute RA at a higher frequency and continue the process until the maximum desired frequency is reached.

This iterative calculation is made using the following three equations. Equation (12) establishes the relationship between RA and  $RR_{pr}$  (see [13], [19] for full description).

This second equation (13) establishes relationship between an intermediate variable  $H$  with a known value of RA at a known frequency ( $f_n$ ). Then the next equation (14) calculates RA at the next frequency ( $f_{n+1}$ ). This process is iteratively repeated until RA reaches the desired frequency.

The RA for different frequencies and  $RR_{pr}$  values can be obtained from [13]:

$$A_r(f_n, RR_{pr}) = \gamma_R(f_n, RR_{pr}) \cdot L_E(f_n, RR_{pr}) \text{ dB} \quad (12)$$

Also, for any specific frequency ranging from 7 to 55 GHz can be obtained from:

$$H(\phi(f_n), \phi(f_{n+1}), A_r(f_n, RR_{pr})) = 1.12 \times 10^{-3} \dots \left( \frac{\phi(f_{n+1})}{\phi(f_n)} \right)^{0.5} \left( \phi(f_n) A_r(f_n, RR_{pr}) \right)^{0.55} \quad (13)$$

$$A(f_{n+1}, RR_{pr}) = A_r(f_n, RR_{pr}) \cdot$$

$$\left( \frac{\phi(f_{n+1})}{\phi(f_n)} \right)^{1-H(\phi(f_n), \phi(f_{n+1}), A_r(f_n, RR_{pr}))} \text{ dB}, \quad (14)$$

$$A_r(\theta, RR_{pr}) = \gamma_R(\theta, RR_{pr}) \cdot L_E(\theta, RR_{pr}) \text{ dB} \quad (15)$$

Where  $A_r(\theta, RR_{pr})$  represents RA for a given value of  $RR_{pr}$ , and propagation angle  $\theta$ , as shown in Figure 7. As a reference, the variables  $L_E$ ,  $\phi$ , and  $\gamma_R$  are described in [13].

This method also has an added advantage by providing high CPU efficiency since we do not have to repeat the entire calculation for each frequency ending with similar results to that for existing ITU-R. It is achieved by



eliminating the accumulated error when compared to that of existing approximated ITU-R solution [13].

The predicted values of RA at any desired location, for different propagation angles,  $RR_{pr}$ , and channel frequency, are important determinants in channel qualities. However, in order to control the satellite channels efficiently, we also need to factor other parameters like gaseous, cloud, fog, and scintillation attenuations as described below.

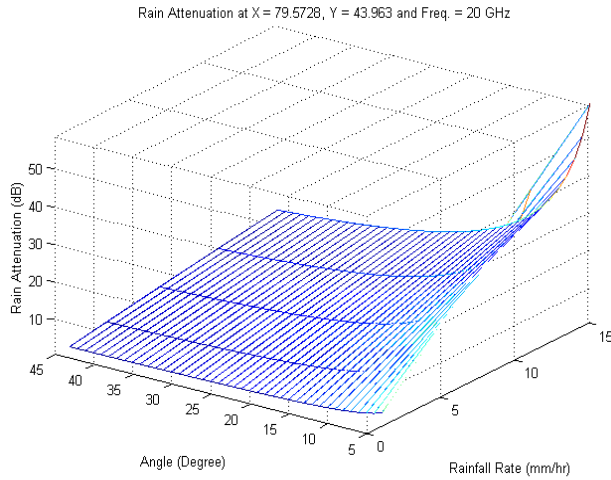


Figure 7. Rain attenuation at South West of King City

### 3.2. Calculating Gaseous Attenuation

In this section, an analytical method for estimating gaseous attenuation has been presented. This has been an extension of the methodology presented in ITU-R P. 676. The slant path attenuation depends on various meteorological conditions created by the distribution of temperature, pressure, and humidity along the transmission path. Thus, the effective path length varies with location, month of the year, height of the station above the sea level, and propagation angle. The gaseous attenuation is calculated using the following steps:

1. Specific attenuation for dry air ( $\gamma_t$ )
2. Specific attenuation for water vapour ( $\gamma_v$ )
3. Equivalent path length for dry air ( $h_t$ )
4. Equivalent path length for water vapour ( $h_v$ ).

Mathematical technique for obtaining the values of these parameters is given below. The calculation of total gaseous attenuation ( $A_g$ ), then follows:

1. Specific Attenuation for the Dry Air ( $\gamma_t$ ):

The attenuation (dB/km) for the frequency ( $f \leq 54$  GHz) is given as:

$$\begin{aligned} \phi(r_{ph}, r_t, a, b, c, d) \\ = r_{ph}^a r_t^b \exp[c(1 - r_{ph}) + d(1 - r_t)] \end{aligned} \quad (16)$$

with

$$\xi_1 = \phi(r_{ph}, r_t, 0.0717, -1.8132, 0.0156, -1.6515)$$

$$\xi_2 = \phi(r_{ph}, r_t, 0.5146, -4.6368, -0.1921, -5.7416)$$

$$\xi_3 = \phi(r_{ph}, r_t, 0.3414, -6.5851, 0.2130, -8.5854) \quad (17)$$

and

$$\gamma_t =$$

$$\left[ \frac{7.2 r_t^{2.8}}{f^2 + 0.34 r_p^2 r_t^{1.6}} + \frac{0.62 \xi_3}{(54 - f)^{1.16 \xi_1} + 0.83 \xi_2} \right] f^2 r_p^2 \times 10^{-3}, \quad (18)$$

#### 2. Specific Attenuation for the Water vapour ( $\gamma_v$ ):

The attenuation  $\gamma_v$  (dB/km) is given as:

$$\begin{aligned} \gamma_w = & \left\{ \frac{3.98 \eta_1 \exp[2.23(1 - r_t)]}{(f - 22.235)^2 + 9.42 \eta_1^2} g(f, 22) + \frac{11.96 \eta_1 \exp[0.7(1 - r_t)]}{(f - 183.31)^2 + 11.14 \eta_1^2} \right. \\ & + \frac{0.081 \eta_1 \exp[6.44(1 - r_t)]}{(f - 321.226)^2 + 6.29 \eta_1^2} + \frac{3.66 \eta_1 \exp[1.6(1 - r_t)]}{(f - 325.153)^2 + 9.22 \eta_1^2} \\ & + \frac{25.37 \eta_1 \exp[1.09(1 - r_t)]}{(f - 380)^2} + \frac{17.4 \eta_1 \exp[1.46(1 - r_t)]}{(f - 448)^2} \\ & + \frac{844.6 \eta_1 \exp[0.17(1 - r_t)]}{(f - 557)^2} g(f, 557) \\ & + \frac{290 \eta_1 \exp[0.41(1 - r_t)]}{(f - 752)^2} g(f, 752) \\ & \left. + \frac{8.3328 \times 10^4 \eta_2 \exp[0.99(1 - r_t)]}{(f - 1780)^2} g(f, 1780) \right\} f^2 r_t^{2.5} \rho \times 10^{-4} \end{aligned} \quad (19)$$

with

$$\eta_1 = 0.955 r_{ph} r_t^{0.68} + 0.006 \rho,$$

$$\eta_2 = 0.735 r_{ph} r_t^{0.5} + 0.0353 r_t^4 \rho \quad (20)$$

$$g(f, f_i) = 1 + \left( \frac{f - f_i}{f + f_i} \right)^2. \quad (21)$$

and

$$h_t = \frac{6.1}{1 + 0.17 r_p^{-1.1}} (1 + t_1 + t_2 + t_3) \quad (22)$$

Where  $ph$ : pressure (hPa),  $r_{ph} = ph/1013$ ,  $r_t = 288/(273 + t)$ ,  $\rho$  water-vapour density ( $g/m^3$ ),  $f$ : frequency (GHz), and  $t$ : mean temperature values ( $^{\circ}C$ ), can be obtained from ITU-R P. 1510 when no adequate temperature data is available.

#### 3. Equivalent Path Length for the Dry Air:

The equivalent height of the dry air is given by:

$$t_1 = \frac{4.64}{1 + 0.066 r_{ph}^{-2.3}} \exp \left[ - \left( \frac{f - 59.7}{2.87 + 12.4 \exp(-7.9 r_{ph})} \right)^2 \right] \quad (23)$$

Where

$$t_2 = \frac{0.14 \exp(2.12 r_{ph})}{(f - 118.75)^2 + 0.031 \exp(2.2 r_{ph})} \quad (24)$$

$$t_3 = \frac{0.0114}{1 + 0.14 r_{ph}^{-2.6}} f \frac{-0.0247 + 10^{-4} f + 1.61 \times 10^{-6} f^2}{1 - 0.0169 f + 4.1 \times 10^{-5} f^2 + 3.2 \times 10^{-7} f^3} \quad (25)$$

and

$$h_o \leq 10.7 r_{ph}^{0.3} \quad (26)$$

with the constraint that:

when  $f < 70$  GHz:

#### 4. Equivalent Path Length for the Water Vapour:

For water vapour, the equivalent height for  $f \leq 350$  GHz is:



$$h_v = 1.66 \left( 1 + \frac{1.39\sigma_v}{(f - 22.235)^2 + 2.56\sigma_v} \right. \\ \left. \dots + \frac{3.37\sigma_v}{(f - 183.31)^2 + 4.69\sigma_v} + \frac{1.58\sigma_v}{(f - 325.1)^2 + 2.89\sigma_v} \right) \quad (27)$$

Where

$$\sigma_v = \frac{1.013}{(1 + \exp[-8.6(r_{ph} - 0.57)])} \quad (28)$$

Notice that water vapour has resonance of (22.235 GHz), (183.31 GHz), and (325.1 GHz) respectively and that attenuation changes with the amount of water vapour in the atmosphere.

• Calculating total gaseous attenuation inclined arrangements of station.

The above method calculates slant path attenuation for water vapour that relies on the knowledge of the profile of water vapour pressure (or density) along the attenuation path.

This section proposes a method to obtain the path attenuation based on surface meteorological data using the cosecant law for a given propagation angle and  $RR_{pr}$  as:

$$A_{Gas}(\theta, RR_{pr}) = \frac{A_\tau + A_v(RR_{pr})}{\sin \theta} \quad (29)$$

where  $A_\tau = h_\tau \gamma_\tau$  and  $A_v = h_v \gamma_v$  dB, and  $\theta \leq 5^\circ$ . Thus, the estimated gaseous values are computed at any desired location, for all ranges of propagation angle and  $RR_{pr}$ , and for any frequency as shown in Figure 8.

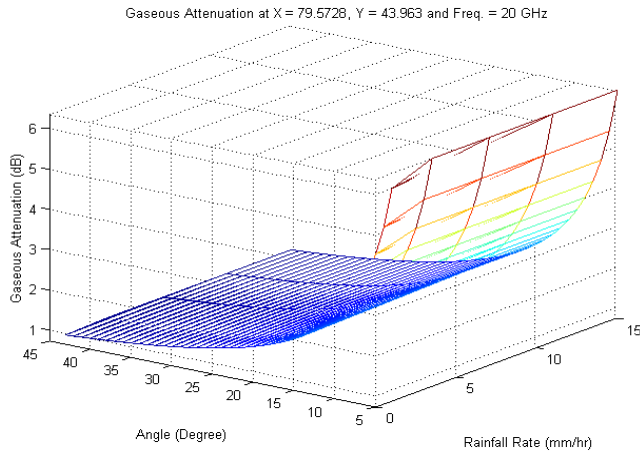


Figure 8. Gaseous attenuation at South West of King City

### 3.3. Calculating Cloud and Fog Attenuations

Cloud and fog can be described as a collection of smaller rain droplets, or alternatively, as different interactions from rain as the water droplet size in fog and cloud is smaller than the wavelength of 3 GHz signals.

The cloud and fog attenuations ( $A_{cf}$ ) can be expressed in terms of  $RR_{pr}$  and propagation angle for a specific frequency and temperature value  $t_k$  (Kelvin), through the following series of equations, culminating into equation (37).

$$D_{p1} = \left( (\epsilon_0 - \epsilon_1) / \left( 1 + (f / f_p)^2 \right) \right) \\ + \left( (\epsilon_1 - \epsilon_2) / \left( 1 + (f / f_s)^2 \right) \right) + \epsilon_2 \quad (30)$$

$$D_{p2} = \left( f \cdot (\epsilon_0 - \epsilon_1) / \left( f_p \cdot \left( 1 + (f / f_p)^2 \right) \right) \right) \\ + \left( f \cdot (\epsilon_1 - \epsilon_2) / \left( f_s \cdot \left( 1 + (f / f_s)^2 \right) \right) \right) \quad (31)$$

$$\eta = (2 + D_{p1}) / D_{p2} \quad (32)$$

$$t_l = 300 / t_k \quad (33)$$

where

$t_k$ : Temperature (Kelvin)

$$\epsilon_2 = 3.51, \epsilon_l = 5.48, \quad (34)$$

and

$$\epsilon_0 = 77.6 + 103.3 (t_l - 1) \quad (35)$$

$$f_s = 590 - 1500 (t_l - 1), \quad (36)$$

and

$$f_p = 20.09 - 142 (t_l - 1) + 294 (t_l - 1)^2 \quad (37)$$

$$K_t = (0.819 f) / (D_{p2} \cdot (1 + \eta^2)) \quad (38)$$

The estimated attenuation due to cloud and fog for a given value is:

$$A_{cf}(\theta, RR_{pr}) = \frac{L_v(pr) \cdot K_t}{\sin \theta} \text{ dB}, \quad (39)$$

Cloud & Fog Attenuation at X = 79.5728, Y = 43.963 and Freq. = 20 GHz

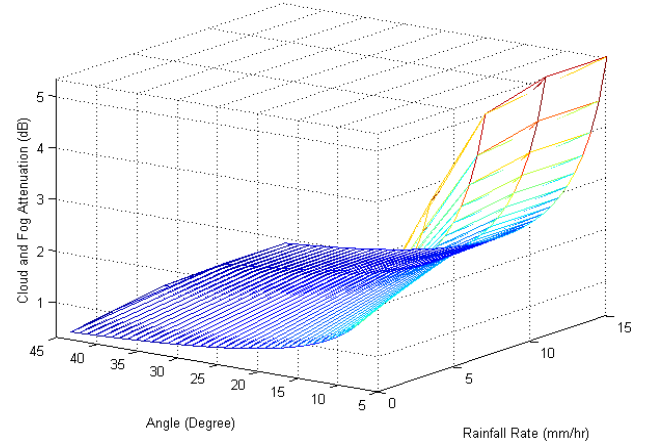


Figure 9. Cloud and Fog attenuations at South West of King City

Scintillation Attenuation at X = 79.5728, Y = 43.963 and Freq. = 20 GHz

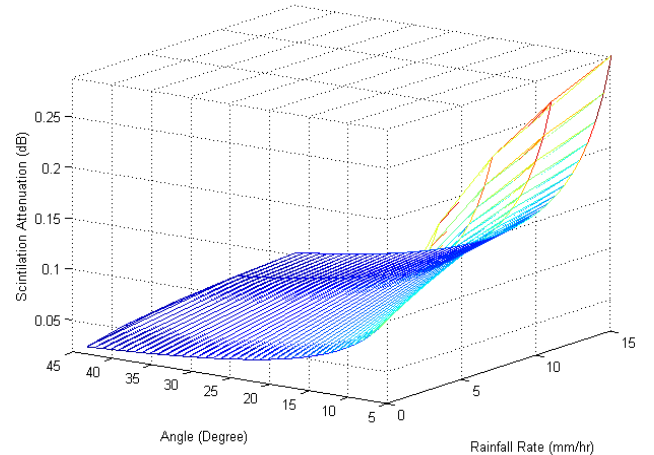


Figure 10. Scintillation attenuation at South West of King City

where  $A_{cf}(\theta, RR_{pr})$  represent cloud and fog attenuations.  $L_v$  ( $\text{kg/m}^2$ ) is the statistics of the total columnar content of liquid water.  $M$  ( $\text{kg/m}^3$ ) is the integration of liquid water

density, along a cross section of  $1 \text{ m}^2$  from surface to top of clouds for a given site. The  $L_v$  is provided from ITU-R for the predicted probability of precipitation ( $pr$ ) based on  $RR_{pr}$ . Refer to [5] to obtain the relation between  $pr$  and  $RR_{pr}$ . In all predicted situations the value of  $pr$  is normally found to be in the range of 0.0001 to 0.5. These attenuations are presented as a function of  $\theta$  and  $RR_{pr}$  at a station in King City has been shown in Figure 9.

### 3.4. Calculating of Scintillation Attenuation

The cumulative distribution of tropospheric scintillation is based on monthly or longer average ambient temperature. This distribution reflects the specific climate condition of the site [5], [39]. In satellite communications, scintillation attenuation results from rapid variations in the signal's amplitude and phase due to changes in the refractive index of the earth's atmosphere. A general technique for predicting this attenuation as a function of  $RR_{pr}$  and propagation angle that is greater than  $4^\circ$  is given here.

Calculate the standard deviation of the signal amplitude,  $\sigma_{ref}$  as:

$$\sigma_{ref} = 3.6 \cdot 10^{-3} + 10^{-4} \cdot N_{wet} \text{ dB}, \quad (40)$$

where  $N_{wet}$ : radio refractivity, given in ITU-R P. 453.

Predicted Atmospheric Attenuation at X = 79.5728, Y = 43.963 and Freq. = 20 GHz

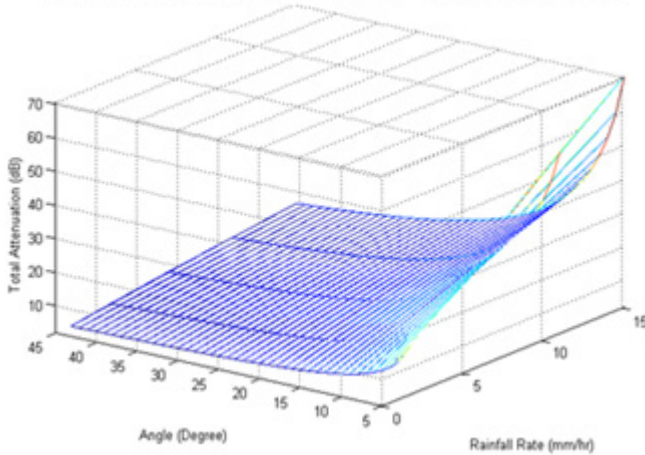


Figure 11. Atmospheric attenuation at South West of King City

Calculate the effective path length  $L$  for the height of the turbulent layer  $h_L$  equal to 1 km:

$$L = \frac{2 h_L}{\sqrt{\sin^2 \theta + 2.35 \times 10^{-4} + \sin \theta}} \text{ meter}. \quad (41)$$

Estimate the effective antenna diameter,  $D_{eff}$ , from the geometrical diameter (meter) of the earth-station antenna ( $D$ ), and the antenna efficiency ( $\eta$ ) (with  $\eta = 0.5$  if unknown), is used as:

$$D_{eff} = \sqrt{\mu} \cdot D \text{ meter}. \quad (42)$$

Calculate the antenna aperture averaging factor from:

$$g(x) = \sqrt{3.86(x^2 + 1)^{1/2} \cdot \sin\left[\frac{11}{6} \arctan\left(\frac{1}{x}\right)\right] - 7.08 x^{5/6}} \quad (43)$$

with

$$x = 1.22 \cdot D_{eff}^2 \cdot (f/L) \quad (44)$$

and

$$\sigma(\theta) = \sigma_{ref} \cdot f^{7/12} \cdot \frac{g(x)}{(\sin \theta)^{1.2}} \quad (45)$$

Calculate time percentage factor,  $a(pr)$ , for the predicted probability of precipitation as follows:

$$a(RR_{pr}) = -0.061 \cdot (\log(pr))^3 \dots 0.072 (\log(pr))^2 - 1.71 \log(pr) + 3.0. \quad (46)$$

Finally, obtain the scintillation attenuation ( $A_s$ ) from:

$$A_s(\theta, RR_{pr}) = a(RR_{pr}) \cdot \sigma(\theta) \text{ dB}. \quad (47)$$

The estimated scintillation attenuation calculated by using (45) on ITU-R data resulted in a set of  $A_s(\theta, RR_{pr})$  values in relation to propagation angle,  $RR_{pr}$ , frequency, and location as shown in Figure 10.

### 3.5. Calculating Total Attenuation

The total attenuation  $A_t$  is made up of two components:

Weather attenuation ( $A_W$ ) and free space attenuation ( $A_0$ ). The weather attenuation ( $A_W$ ) is calculated from the four constituent attenuations calculated in preceding subsections. They are:

1.  $A_r(\theta, RR_{pr})$ : rain attenuation, as estimated in (15).
2.  $A_g(\theta, RR_{pr})$ : gaseous attenuation due to water vapour and oxygen, as estimated in (29).
3.  $A_{cf}(\theta, RR_{pr})$ : cloud and fog attenuations, as estimated in (39).
4.  $A_s(\theta, RR_{pr})$ : attenuation due to tropospheric scintillation, as estimated in (47).

Given these four attenuations, the total weather attenuation  $A_W(\theta, RR_{pr})$ , can be calculated from [5], [8], and [13]:

$$A_W = A_{Gas} + \sqrt{(A_{Rain} + A_{Cloud \& Fog})^2 + A_{Scintillation}^2} \quad (48)$$

The results with the available measurement data for all latitudes for the prediction of wide  $RR_{pr}$  ranges and propagation angle are shown in Figure 7, Figure 8, Figure 9, Figure 10, and Figure 11. The second component of attenuation is caused by free space [36, 37]. We call the loss that occurs in free space free space attenuation.

Table 3. Antenna Noise temperature  $T_a$  (Kelvin)

Directional satellite antenna	Earth from space	290 K
Directional terminal antenna	Space from earth at $90^\circ$ elev.	3 – 10 K
	Space from earth at $10^\circ$ elev.	$\approx 80 \text{ K}$
	Sun (1...10 GHz)	$10^5 \dots 10^6 \text{ K}$
Hemispherical terminal antenna	At night	290 K
	Cloudy sky	360 K
	Clear sky with sunshine	400 K

The free space attenuation,  $A_0(f)$ , is obtained as follows:

$$A_0(f) = (4\pi \cdot d/\lambda)^2, \quad (49)$$

Where  $d$  is the distance between transmitter and receiver and the wavelength  $\lambda = c/f$ . It would be significant to note that a free space is space with nothing at all in it.

This phenomenon does not exist in the known universe but interstellar space is a good approximation. The most important four features of free space are its uniformity

everywhere, absence of electrical charge, no current flowing through it, and its infinite extent in all directions [40], [41].

That we have obtained atmospheric attenuation and free space loss, the total attenuation ( $A_t$ ) can be calculated from the following relation:

$$A_t(\theta, RR_{pr}) = A_W(\theta, RR_{pr}) + A_0(f), \quad (50)$$

Where  $A_t(\theta, RR_{pr})$  is the total attenuation,  $A_W(\theta, RR_{pr})$  is the atmospheric attenuation described in (48)(48), and  $A_0(f)$  is the free space loss described in (49).

A three dimensional relationship for these attenuations with respect to propagation angle and  $RR_{pr}$  is presented in Figure 12.

These attenuations, for systems running at frequencies above 10 GHz- especially those operating with low propagation angles and/or margins, must be considered along with the effect of multiple sources of simultaneous occurring.

This method provides a useful general tool for scaling atmospheric attenuations according to these parameters.

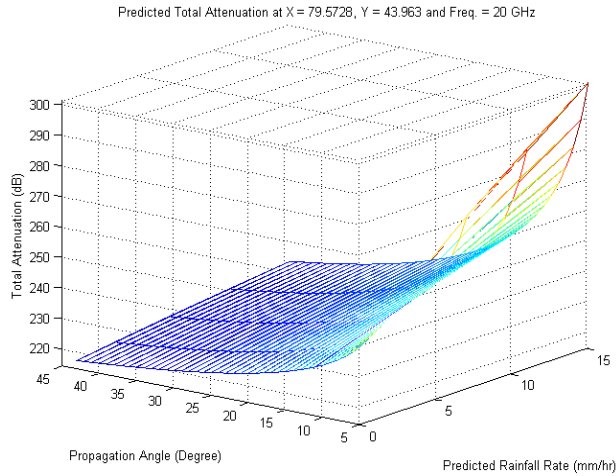


**Figure 12.** Predicted total attenuation at South West of King City

Also, it helps to provide designers with a perceptible view of approximated different attenuation values that can be computed at any desired location, for different frequencies, and for wide ranges of  $RR_{pr}$  and propagation angles. The outcome becomes a key factor in diagnosing, adjusting and improving satellite signal power, modulation and coding schemes, monitored and controlled altogether by a powerful and efficient intelligent-based attenuation countermeasure system.

We found that practically the prediction of total attenuation obtained in this way is respectable approximation. The total attenuation is used to calculate SNR, which is then used by the IWACS in determining channel quality and subsequently adjusting satellite propagation parameters as described in the next section.

### 3.6. Relating Total Attenuation with Signal to Noise Ratio (SNR)

SNR is a measure of signal strength for satellite signal relative to attenuations and background noise, usually measured in decibels (dB) [41]. The signal energy ( $E_s$ ) to noise power spectral density ( $N_0$ ) per symbol is calculated

from the knowledge that  $E_s = C \cdot T_s = C \cdot R_s$ , where  $C$  is signal power,  $T_s$  is symbol duration, and  $R_s$  transmission rate.

$$\frac{E_s}{N_0} = \frac{C}{N_0} \cdot T_s = \frac{C}{N_0} \cdot \frac{1}{R_s}. \quad (51)$$

Where thermal noise power spectral density  $N_0 = K_b \cdot T$ , and  $K_b$  (Boltzmann constant) =  $1.38 \cdot 10^{-23}$  Ws/K = 228.6 dBWs/K.

$$T \text{ (effective noise temperature)} = T_a + T_r \quad (52)$$

Where  $T_a$  is noise temperature of the antenna as represented in Table 3, and

$$T_r \text{ (noise temperature of the receiver)} \\ = (10^{N_r/10} - 1) \cdot 290. \quad (53)$$

In the above equation the Noise Figure ( $N_r$ ) for a low-noise amplifier is found to be in the range of 0.7 to 2 dB. The above equations can now be combined as:

$$\frac{C}{N_0} = \frac{C}{K_b \cdot T} = \frac{P_r}{K_b \cdot T} = \frac{P_t \cdot G_t}{A_t} \cdot \frac{G_r}{K_b \cdot T} \quad (54)$$

Where  $P_t$  and  $P_r$  are transmitter and receiver power, and  $G_t$  and  $G_r$  are antenna gain at transmitter and receiver sides respectively. Therefore,

$$\frac{C}{N_0} = P_t + G_t - A_t + G_r - K_b - T \quad (55)$$

$$\frac{E_s}{N_0} (A_t, P_t) = P_t + G_t - A_t + G_r - K_b - R_s \quad (56)$$

It should be noted that the SNR estimation of (54) will be optimized by the virtue of having better estimation of  $A_t$  through (56).

## 4. Simulation Results and Discussions

### 4.1. Simulation Environment and Implementation

The mathematical solution for finding any weather attenuation and utilizing that information to improve signal quality in satellite networks were tested in a simulated system named IWACS. The system monitors channel qualities and applies counter measures, which involves controlling of power, frequency, propagation angle, modulation, coding, and data rate.

The outcome is the evolution in signal fidelity, especially above 10 GHz, through reduction in digital transmission errors.

In this section, the architecture of the IWACS is briefly mentioned. Details are avoided because the material presented in earlier section has been the main focus of this article.

The IWACS was simulated in Matlab simulations version 7.10.0 running on i7 - 2630QM, 2.00 GHz CPU and 6.00 GB RAM. A special module was written to read weather data from Environment Canada supplied in a specially formatted text stream and converted into a three hour sliding window of moving weather data always preceding the present moment.

Software modules were written to extract propagation

related parameters shown in Figure 5 for the location from ITUR supplied data. Algorithm for predicting the RR based on Markov theory with fixed-duration weather data was written.

Also, the IWACS used heuristic algorithms that employed field inputs in problem solving, learning and discovery. The system adhered to formalized knowledge representations schemes practiced in the industry, and machine learning techniques, to reach optimal decision in dealing with different atmospheric conditions [5], [8], [16], [42], and [43]. The key feature of the IWACS is that it adjusts to signal variations with a fast response time. In accomplishing this, the employed technique used feedback of SNR values from the receiving end of the channel and uses that knowledge to mitigate future weather attenuations, thus preventing them from actually manifest in the channels. This proactive approach to the adjustment of signal characteristics is what makes the system meet end-to-end QoS requirements. The core architecture of the IWACS is shown in Figure 13, where it may be noted that it consists of four control blocks, the first control block, the second control block, the third control block, and the fourth control block, a feedback loop and counter iteration, along with a special module called decision support system (DSS). This figure illustrates the interrelationships of various blocks involved in tuning propagation characteristics of a communication

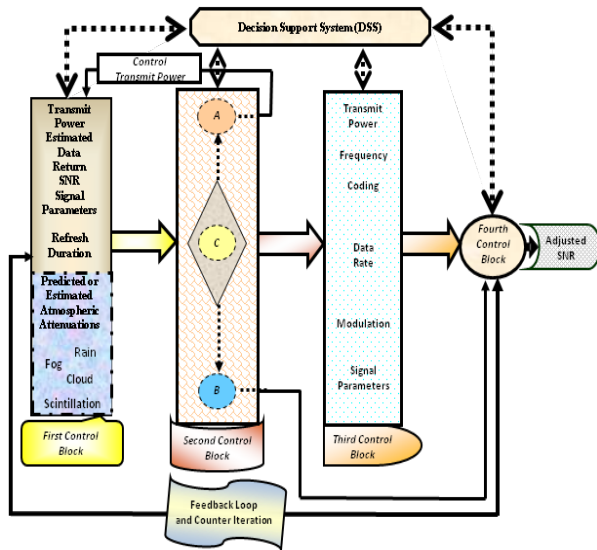


**Figure 13.** Intelligent weather aware system for satellite networks

The first control block collects vital data like propagation angle, frame size, frequency, transmit signal power, and weather data. Based on these data, it computes atmospheric attenuation and SNR for the following time period. This is where the bulk of the techniques explained in earlier sections are employed.

The second control block compares the differences between the estimated SNR and the minimum SNR values sought to maintain a desired level of QoS, usually set by system's designers based on experience. These comparisons lead to one of three different possible outcomes  $\{A, B, \text{ or } C\}$  as shown in Figure 13. The first outcome  $\{A\}$ , is for

estimated SNR values smaller than the threshold level. In this case the DSS will decide to increase transmit power up to a maximum limit of  $-30 \text{ dB}$  ( $0 \text{ dBm}$ ). The second outcome  $\{B\}$ , is where estimated SNR values equal to or exceed the threshold level. The DSS will be satisfied and will jump to the last block. The third outcome  $\{C\}$ , is for estimated SNR smaller than the threshold level even after increasing the transmit power to its maximum value. The DSS will go to the next block for selecting a combination of transmission characteristics.

In the third control block, based on adjusted SNR value, the DSS will opt for the adjustment of other parameters such as data rate, frequency, modulation, and coding values. If the threshold level value can be reached by using any of the different variable combinations, then the DSS will decide to move to the last block for the final decision. This block employs an aid similar to Table 4 in making these decisions, which are prepared based on field experience and expert suggestions.

**Table 4.** Forward link modes and performance at South West of King City for propagation angle =  $45 \text{ Degrees}$  and frequency =  $20 \text{ GHz}$

Modulation	LPC Code Identifier	Es/N0 Estimated Values [dB]	Transmitted Power [dB]	Weather Attenuations [dB]
QPSK	2/3	12.37	-55	214.36
QPSK	4/5	5.90	-60	223.46
8PSK	2/3	1.2	-62	221.13
8PSK	8/9	4.86	-58	218.69
16PSK	8/9	21.10	-57	216.23

The fourth control block interacts with the remote end of the channel and determines the current SNR. It then feeds the current SNR value to the input block so that the system's real time state is appropriately monitored. This in turn helps iteratively adjust the channel state.

In case a satisfactory SNR is not achieved through different combinations, the control system goes back to first control block through feedback and counter iteration block to re-adjust the parameters (as explained earlier) and comes to re-work with the tables according to DSS decision, until a satisfactory value is reached at which the procedure will stop. In case significant improvement is not achieved, the system will abandon the process after a set number of iterations and gives a warning to the operator. Whereas, the number of iteration can be set by system's designers based on the specific location.

The SNR and other measured parameters are fed to the DSS block to help make the decision to maintain QoS and satisfy SLAs. The DSS and its network optimization blocks are depicted in Figure 14.

The periodically-computed attenuation keeps updating the knowledge input to the DSS, which is constructed from specific classes of algorithms that take experiential decision inputs from the user so that they could be factored in decision-making activities. Typical information that a DSS might gather and present would be:



a- Accessing current information assets such as knowledgebase, satellite parameters, and triggering of periodic query

b- Maintaining the database of different combinations of channel parameters known to give acceptable system performance. The other blocks can then find the right combinations with the aid of DSS.

Thus, the IWACS minimizes the attenuation effect and maximizes the channel robustness and efficiency by improving SNR. Such improvement in turn improves QoS. The ability to better predict rain attenuation for different weather conditions and operational frequencies makes the quest for improved QoS a reality.

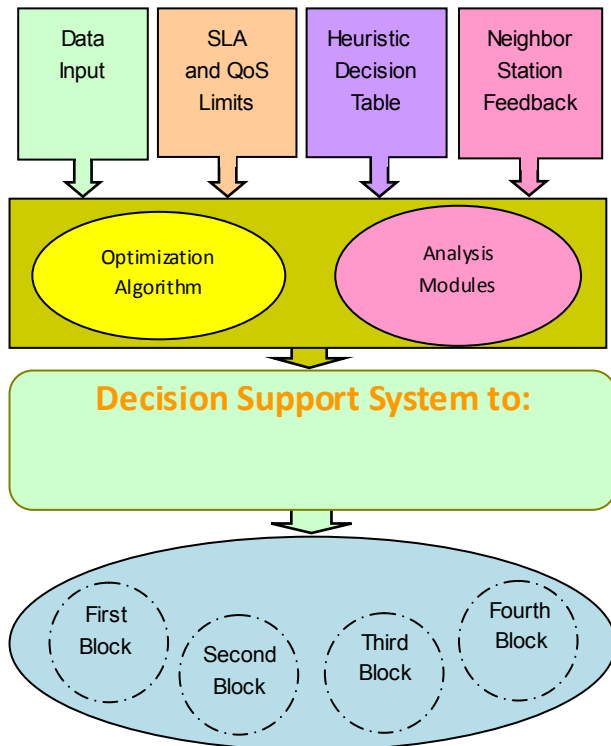


**Figure 14.** Network optimization Decision Support System (DSS)

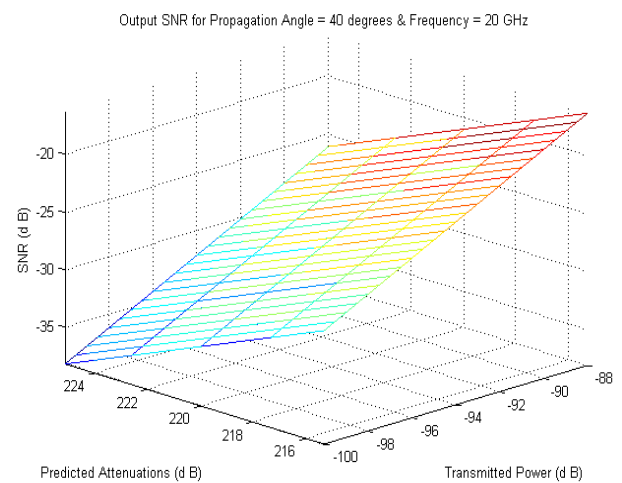
## 4.2. Results

The system, built on the foundation of the above mentioned principles, was found to deliver noteworthy improvements in the performance of satellite networks.

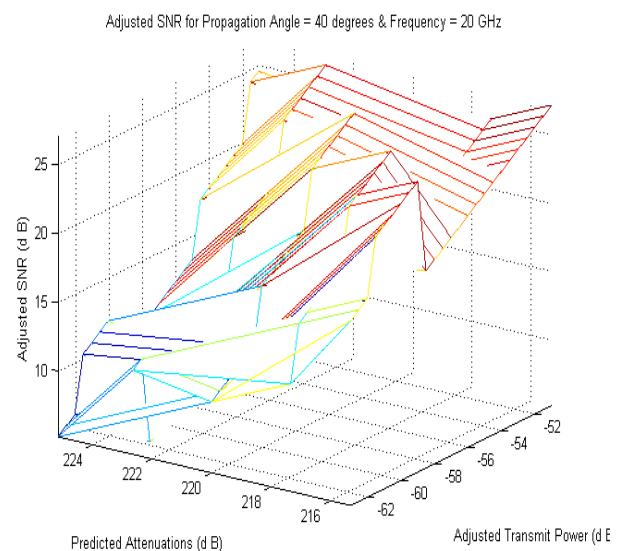
The system monitored the SNR at the receiving end of the channels, compared it with a threshold, and searched for a blend of available power, frequency, propagation angle, coding, transmission rate, and modulation in response to predicted channel attenuation. It then attempted to maintain a desired level of SNR as shown in Figure 12, Figure 13, Figure 14, Figure 15, and Figure 16. Such maintenance required the aid of an expanded form of Table 4 for selecting the right combination of propagation parameters.

Figure 15 and Figure 16 compare the SNR before and after the techniques discussed in this paper are put to use for making improved system performance. These figures represent cases when SNR fell between  $(-39 \sim -16)$  dB, and transmit power from  $(-100 \sim -88)$  dB before

intelligent decision mechanism was turned on. The improvements made in SNR and transmit power level were significant after the IWACS was allowed to operate under the same conditions. The SNR improved to  $(5 \sim 27)$  dB and the transmit power level ranged from  $(-63 \sim -51)$  dB. Both cases were subjected to identical weather conditions where total attenuation due to weather ranged from  $(215 \sim 225)$  dB for a frequency of 20 GHz at 40 degree propagation angle. Note that the system was able to bring the upper limit of transmit power to less than the maximum allowed of -30 dB. Any time this limit is reached, signal parameters are re-adjusted to prevent uncontrolled signal transmission as shown in Figure 16 and Table 4. It should be noted that the improvements in channel performance made by the scheme are significant.



**Figure 15.** Output SNR at South West of King City channel



**Figure 16.** Adjusted output SNR at South West of King City

## 5. Conclusions

Precipitation, gaseous formation, cloud, fog, and scintillation cause attenuation of satellite signals. These attenuations become especially prominent at frequencies

above Ku band. Such attenuation makes it difficult to provide agreed upon QoS by satellite networks unless special mitigation measures are devised to counter weather effects. Such control systems could be optimized to its most effective status if we had the best possible techniques for predicting channel attenuation due to weather related factors. This paper presents a technique for predicting channel attenuation based on real-time weather data and the use of the Markov theory. The results thus obtained, are found to be able to make significant improvement over the techniques known thus far. This technique positively contributes to QoS maintenance by allowing for better tuning and adaptation of signal propagation parameters such as frequency, power, propagation angle, modulation, coding, and transmission rate with changing weather conditions. The paper also introduces a three dimensional relationship model between attenuation, propagation angle, and  $RR_{pr}$  with an implication that for a given atmospheric condition, the signal attenuation could be predicted with much improved accuracy than the techniques known to us. An IWACS, which controls modulation, coding, transmission power, frequency, propagation angle, and transmission rate to improve channel robustness, is briefly described. It is believed that the technique presented here can be of significant interest to research and development community interest in improving the throughput of satellite networks.

## ACKNOWLEDGEMENTS

This work is supported by the Deanship of Scientific Research (DSR) at King Fahd University of Petroleum & Minerals (KFUPM) through project No. JF111005.

## REFERENCES

- [1] R. K. Crane, "Prediction of the effects of rain on satellite communication systems," *Proc. of the IEEE*, vol. 65, pp. 456–474, March 1977.
- [2] F. Haidara, A. Dissanayake, and J. Allnutt, "A prediction model that combines rain attenuation and other propagation impairments along Earth-satellite paths," *IEEE Trans. on Antennas & Propagation*, vol. 45, pp. 1546–1558, Oct. 1977.
- [3] ITU-R, Rain height model for prediction methods. Radio wave propagation, International Telecommunication Union. Rec. P.837-4, ITU-R, Fascicle, Geneva, 2001.
- [4] D. V. Rogers, L. J. I. Jr., and F. Davarian, "System requirements for ka-band Earth-satellite propagation data," *Proc. of the IEEE*, vol. 85, no. 6, pp. 810–820, 1997.
- [5] K. Harb, A. Srinivasan, B. Cheng, and C. Huang, "Intelligent weather aware scheme for satellite systems," in *Proc. IEEE ICC'08*, May 2008.
- [6] J. Pelton, "The start of commercial satellite communications [History of communications]," *IEEE Communications Magazine*, vol. 48, no. 3, pp. 24–31, 2001.
- [7] L. J. Ippolito, "Propagation effects and system performance considerations for satellite communications above 10 GHz," *Proc. of the IEEE*, vol. 1, pp. 86–91, Dec. 1990.
- [8] K. Harb, F. R. Yu, P. Dakhal, and A. Srinivasan, "Performance improvement in satellite networks based on markovian weather prediction," in *Proc. IEEE GlobCom'10*, Dec. 2010.
- [9] A. A. Aboudebra, K. Tanaka, T. Wakabayashi, S. Yamamoto, and H. Wakana, "Signal fading in land-mobile satellite communication systems: Statistical characteristics of data measured in Japan using ETS-VI," *Microwave, Antennas & Propagation*, vol. 146, pp. 349–354, Oct. 1999.
- [10] L. J. Ippolito and T. A. Russell, "Propagation considerations for emerging satellite communications applications," *Proc. of the IEEE*, vol. 81, pp. 923–929, June 1993.
- [11] L. Mathy, C. Edwards, and D. Hutchison, "Principles of QoS in group communications," *Telecommunication Systems*, vol. 11, no. 1-2, pp. 59–84, 1999.
- [12] ITU-R, "Attenuation due to clouds and fog," Radio wave propagation, International Telecommunication Union Recommendation ITU-R P.840-3, 1999.
- [13] K. Harb, A. Srinivasan, B. Cheng, and C. Huang, "Prediction method to maintain QoS in weather impacted wireless and satellite networks," in *Proc. SMC*, Oct. 2007.
- [14] ITU-R, Specific attenuation model for rain for use in prediction methods. Radio wave propagation, International Telecommunication Union. Rec. P.838-3, ITU-R, Fascicle, Geneva, 2003.
- [15] K. Harb, F. R. Yu, P. Dakhal, and A. Srinivasan, "A decision support scheme to maintain QoS in weather impacted satellite networks," in *Proc. AIAA Atmospheric and Space Environments Conference'10*, (Toronto, ON, Canada), Aug. 2010.
- [16] Telesat Canada, "ISS (Intelligent Satellite Service) Research and Development," website: <http://www.telesat.ca>, last accessed date March 2012.
- [17] J. S. Mandeep, Y. Y. Ng, H. Abdullah, and M. Abdullah, "The study of rain specific attenuation for the prediction of satellite propagation in Malaysia," *Journal of Infrared, Millimeter and Terahertz Waves*, vol. 31, no. 6, pp. 681–689, 2010.
- [18] ITU, "Radio communication sector (ITU-R) home," website: <http://www.itu.int/ITU-R>, last accessed date April 2012.
- [19] K. Harb, A. Srinivasan, B. Cheng, and C. Huang, "QoS in weather impacted satellite networks," in *Proc. IEEE Pacific Rim Conference on Communications, Computers and Signal Processing*, (Victoria, B.C., Canada), Aug. 2007.
- [20] C. I. Christodoulou, S. C. Michaelides, M. Gabella, and C. S. Pattichis, "Prediction of rainfall rate based on weather radar measurements," in *International Joint Conference on Neural Networks IJCNN*, (Budapest, Hungary), July 2004.
- [21] J.-C. Hsieh, H.-P. Lin, and C. Yang, "A two-level, multistate markov model for satellite propagation channels," *Proc. IEEE VTC*, vol. 4, pp. 3005–3009, May 2001.
- [22] J. A. Garcia-Lopez, J. M. Harnando, and J. M. Selga, "Simple

- rain attenuation prediction method for satellite radio links," IEEE Trans. on Antennas & Propagation, vol. 36, pp. 444-448, March 1988.
- [23] U. C. Fiebig, "Modeling rain fading in satellite communications links," in Proc. IEEE VTC'99, vol. 3, pp. 1422-1426, Sept. 1999.
- [24] E. E. Altshuler, M. A. Gallop, Jr., and L. E. Telford, "Atmospheric attenuation statistics at 15 and 35 GHz for very low elevation angles," Radio Science, vol. 13, no. 5, pp. 839-852, 1978.
- [25] S. D. Slobin, "Microwave noise temperature and attenuation of clouds: Statistics of these effects at various sites in the United States, Alaska and Hawaii," Radio Science, vol. 17, no. 6, pp. 1443-1454, 1982.
- [26] L. Saloff-Coste, Lectures on finite Markov chains. In Lectures on probability theory and statistics (Saint-Flour, 1996), vol. 1665. Springer, Berlin, 1997.
- [27] V. Network, "Bilinear interpolation definition." website: <http://www.pcmag.com/encyclopedia-term/0,1237,t=bilinear+interpolation&i=38607,00.asp>, last accessed date March 2012.
- [28] R. McLeod and M. L. Baart, Geometry and Interpolation of Curves and Surfaces. Cambridge University Press, July 1998.
- [29] D. A. Sanchez-Salas and J. L. Cuevas-Ruiz, "N-states channel model using Markov Chains," Proc. of Electronics, Robotics and Automotive Mechanics Conference, pp. 342 - 347, Oct. 2007.
- [30] W. Suozhu, L. Haifang, and H. Zhaohui, "Application of Markov Chains prediction model in product layout optimization," International Forum on Computer Science-Technology and Applications (IFCSTA)'09, vol. 3, no. 10, pp. 243-246, 2009.
- [31] V. Network, "VSAT network types." website:[http://www.comsys.co.uk/wvm\\_mn.htm](http://www.comsys.co.uk/wvm_mn.htm), last accessed date Feb. 2012.
- [32] K. M. S. Murthy, J. Alan, J. Barry, B. G. Evans, N. Miller, R. Mullinax, P. Noble, B. O'Neal, J. J. Sanchez, N. Seshagiri, D. Shanley, J. Stratigos, and J. W. Warner, "VSAT user network examples," Communication Magazine, vol. 27, pp. 50-57, May 1989.
- [33] D. Chakraborty, "VSAT communications networks - An overview," Communication Magazine, vol. 26, pp. 10-24, May 1988.
- [34] L. P. Seidman, "Satellites for wideband access," Communication Magazine, vol. 34, pp. 108-111, Oct. 1996.
- [35] ITU-R, Propagation data and prediction method required for the design of Earth-space Telecommunication systems. Radio wave propagation, International Telecommunication Union. Rec. P.618-7, ITU-R, Fascicle, Geneva, 2001.
- [36] L. A. Hoffman, H. J. Wintroub, and W. A. Garber, "Propagation observations at 3.2 millimeters," Proc. of the IEEE, vol. 54, pp. 449-454, June 2005.
- [37] K. Harb, F. R. Yu, P. Dakhil, and A. Srinivasan, "An intelligent QoS control system for satellite networks based on markovian weather," in Proc. IEEE VTC'08, Sep. 2010.
- [38] Y. Karasawa, K. Yasukawa, and M. Yamada, "Tropospheric scintillation in the 14/11-GHz bands on Earthspacepaths with low elevation angles," IEEE Trans. on Antennas & Propagation, vol. 36, pp. 563-569, March 1988.
- [39] G. Maral and M. Bousquet, Satellite Communications Systems. John Wiley & Sons Ltd, UK, 1993.
- [40] E. Lutz, M. Werner, and A. Jahn, Satellite Systems for Personal and Broadband Communications. Springer, New York, 2000.
- [41] Y. Leung, Intelligent spatial decision support systems. Springer Verlag, New York, 1997.
- [42] L. J. Bannon, "Group decision support systems: An analysis and critique," In Proceedings of 5th European Conference on Information Systems, pp. 526-539, June 1997.